Three-dimensional imaging of dielectric patterns in electrohydrodynamic convection of a nematic liquid crystal

N. Gheorghiu,[1,2,*] I. I. Smalyukh,[1] O. D. Lavrentovich,[1] and J. T. Gleeson[2]
[1]*Liquid Crystal Institute, Kent State University, Kent, Ohio 44242-0001, USA*
[2]*Department of Physics, Kent State University, Kent, Ohio 44242-0001, USA*
(Received 22 June 2006; published 5 October 2006)

The transition from surface to bulk normal dielectric rolls in a nematic liquid crystal is imaged by fluorescence confocal polarizing microscopy. The three-dimensional director structure and the liquid flow are scanned in both the layer plane and the transverse plane. Two systems of small-scale convective flow are formed, one at each electrode. Strong anchoring makes director oscillations difficult and charges accumulate by the Carr-Helfrich mechanism. The middle region is a structureless convection where the director oscillates with the frequency of the applied voltage. The small-scale flow eventually fills the cell from one electrode to the other as one system of thin and elongated rolls. The true dielectric mode is not a director pattern, rather a surface flow instability.

DOI: 10.1103/PhysRevE.74.041702 PACS number(s): 61.30.−v, 47.54.−r, 47.20.−k, 33.50.−j

I. INTRODUCTION

Liquid crystals [1,2] (LCs) continue to be very attractive both for their display applications [3–6] and for studying pattern formation on a convenient scale [7–11]. In particular, electrohydrodynamic instability (EHI) in nematic liquid crystals (NLCs) provides many interesting situations for studying pattern formation in an anisotropic dissipative system [12,13]. The standard configuration for EHI is when a NLC thin film is confined between two parallel conducting glass plates where it has a planar (homogeneous) alignment. The rotational symmetry of the NLC director is broken in the layer plane *xy* and, therefore, the system is anisotropic in this plane. When an alternating voltage is applied across the layer plane, the dynamics of the director field, the fluid flow, and the electric charge field exhibit two different modes [13–15]. In the low-frequency or conductive mode, the director and the fluid flow are stationary, while the charge follows the applied alternating current (ac) drive. While increasing the threshold voltage (cell gap independent), the system instabilities go from oblique rolls to normal rolls, to fluctuating rolls, and finally to traveling rolls. The Carr-Helfrich (CH) mechanism [16,17] explains the development of EHI as a result of the coupling between the system orientational anisotropy and its anisotropic conductivity. Using the shadowgraph technique [18], various patterns are optically revealed. The first instability from the quiescent to the convective state can be to oblique rolls followed by normal rolls (NRs), having the orientation oblique and, respectively, normal to the director axis. Their periodicity is about the cell gap d. NRs are also referred to as the Williams-Kapustin domains [19,20]. The aspect ratio is of the order of 10^2-10^3, and therefore boundary conditions are not important. Above the cutoff frequency f_c, there is the so-called dielectric mode. The first instability is to normal dielectric rolls (NDRs) followed by the defect-mediated, chevron(like) director pattern. Here, the situation is reversed: the charge distribution is stationary, while the director and the flow oscillate with the frequency of the applied voltage. The conductive mode is, therefore, director dominated, while the dielectric mode is charge dominated. In the dielectric mode there is a field threshold, i.e., the onset voltage scales with d. The pattern wavelength decreases with increasing frequency and it is significantly smaller than that of the conductive pattern.

In order to understand pattern selection in the EHI of NLCs, one would like to find where and on what scale convection first starts. These are still challenging questions, although they have been specifically raised a few decades ago [21,22]. Experiments in which the direction of the applied electric field was either parallel [23–26] or transverse [27,28] to the direction of optical observation revealed the dielectric instability localized at the cell electrodes. The observation of the true dielectric mode can be difficult, because it can be easily confused with the isotropic mode of EHI [15] that can be observed in any ordinary fluid. In thick cells, the inertial terms in the Navier-Stokes equations play an important role. Surface vortices located at the electrodes do not rotate with the field frequency, but much more slowly ($f_{vort} \approx 1$ Hz [29]). During this time, the dielectric torque applies a shear rate on the director field [30] at the same frequency as that of the driving voltage. The isotropic mode is insignificant in thin samples, at low frequencies, and for a high-viscosity material [15]:

$$1/\tau_D \ll \omega \ll \pi^2 \alpha_{av}/\rho_{av} d^2 \qquad (1)$$

where $\tau_D = \epsilon_0 \epsilon_\parallel / \sigma_\parallel$ is the dielectric relaxation time, $\omega = 2\pi f$, with f the frequency of the ac drive, α_{av} is the average Leslie

Mischung 5

FIG. 1. Molecular structure of the nematic liquid crystal Mischung 5.

*Present address: Department of Physics, Bryn Mawr College, Bryn Mawr, Pennsylvania 19010. Electronic address: ngheorghiu@brynmawr.edu

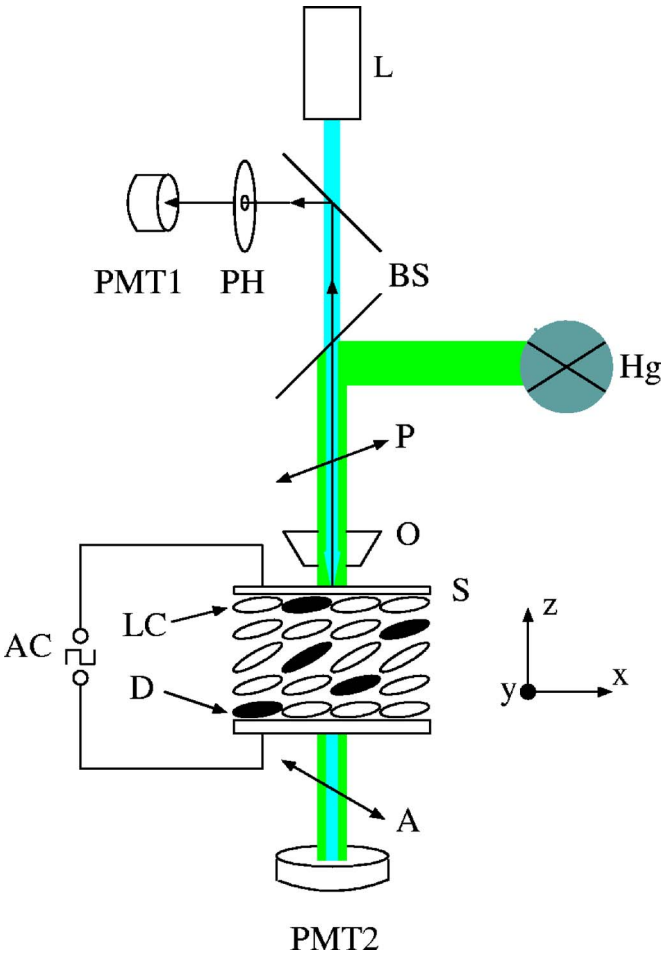

FIG. 2. (Color online) Experimental setup for scanning 3D patterns of orientational order and the liquid flow in a liquid crystal by fluorescence confocal polarizing microscopy. L=Ar laser (λ =488 nm); BS=beam splitter; Hg=mercury lamp; P=polarizer; O=microscope objective; S=sample; LC=liquid crystal molecule; D=dye molecule; A=analyzer; PH=pinhole; PMT1(2) =photomultiplier(s); AC=alternating current (square wave) function generator.

coefficient, whose value can be increased by lowering the temperature, ρ_{av} is the average density, and d is the layer thickness. Indirect experimental evidence [31], using a twisted cell geometry in a laser scattering setup [32], found that in the dielectric mode the fluid flow has a three-layer structure, consisting of two layers of antiparallel vortices located near the electrodes, and structureless convection in the cell middle. This kind of structure for the fluid flow was actually obtained from calculations and predicted to be the precursor of turbulence [33]. There is no surprising coincidence here, since it is the stabilizing dielectric torque (for a material with $\epsilon_a<0$) that suppresses the convective instability at high voltages in the conductive mode or at high frequencies in the dielectric mode. Despite all this, a full understanding of the dielectric mode is still missing. The most discussed issue is, still, whether the patterns are bulk instability or rather surface rolls located at the electrodes. Polarizing microscopy in the transverse observation [26] showed small-scale stationary flow in the form of growing plumes located near electrodes, and breakdown of convection in the cell middle. Test particles were observed to execute an oscillatory motion directed along the applied field, indicating the presence of small vortices [21,29] and a nonuniform field distribution near the electrodes [34].

The high-frequency dielectric mode of the EHI exhibits effects not described by the standard model (SM) [35]. The isotropic flow instability represents a challenge for the SM since it can be obtained in any ordinary (isotropic) liquid. The instability is driven by inverted charge gradients in thin Debye layers near the electrodes [15] and this is something that the SM cannot explain. While both the dielectric and the isotropic modes are potentially active mechanisms, only one is achieved under given experimental conditions. In order to observe the dielectric mode only, one should increase the threshold for the isotropic flow instability (for instance, by increasing the LC viscosity), and/or lower the threshold for the dielectric mode (by increasing the anisotropy in the electrical conductivity) [21]. The first condition can be satisfied, for instance, by choosing to observe the instability at lower temperatures. The choice of a low-conductive (pure) material is also beneficial. In strongly conductive NLCs, the lowest threshold corresponds to the inertial branch of the CH instability, and broad domains are observed [22].

Previous work explored the formation of NDRs, treating LCs as ordinary liquids. The interplay between the LC director and the fluid flow leads to effects not observed in ordinary (isotropic) liquids. In particular, EHIs are more complex than in isotropic fluids. The main purpose of the present work is to bring evidence that the true dielectric mode is, rather than a director pattern, surface flow instability. We have employed fluorescence confocal polarizing microscopy (FCPM) [36,37] to image the three-dimensional (3D) director structure and the fluid flow in a NLC undergoing the EHI.

II. EXPERIMENTAL SETUP

The NLC used in the experiments was Mischung 5 (purified, thus low conductive), a chemically stable, four-component mixture of alkyloxyphenyl-alkyl(oxy)benzoates: 4-hexyloxyphenyl-4′-methoxybenzoate ($\bar{1}O\bar{6}$) 22.0%, 4-octyloxyphenyl-4′-penthyloxybenzoate ($\bar{5}O\bar{8}$) 30.3%, 4-heptyloxyphenyl-4′-hexyloxybenzoate ($\bar{6}O\bar{7}$) 13.3%, and 4-butyloxyphenyl-4′-hexylbenzoate ($6O\bar{4}$) 34.4%. The molecular structure is shown in Fig. 1. The material parameters [38–40] are strongly temperature dependent, thus offering the possibility for a whole range of experiments carried on at fixed frequency. Relevant for EHI is the negative dielectric anisotropy ϵ_a and a positive electric conductivity anisotropy σ_a. Fluorescent material was obtained by doping Mischung 5 at 0.016 wt % with the electrically neutral dye n,n'-bis(2,5-di-tert-butylphenyl)-3,4,9,10-perylenedicarboximide (BTBP) [41].

The optical scanning method used, FCPM, visualizes the intensity of polarized fluorescence light emitted by the dye molecules as the liquid crystal molecules align them. The fluorescence signal peak occurs when the transition dipole of the dye molecules is parallel to the polarization of the input

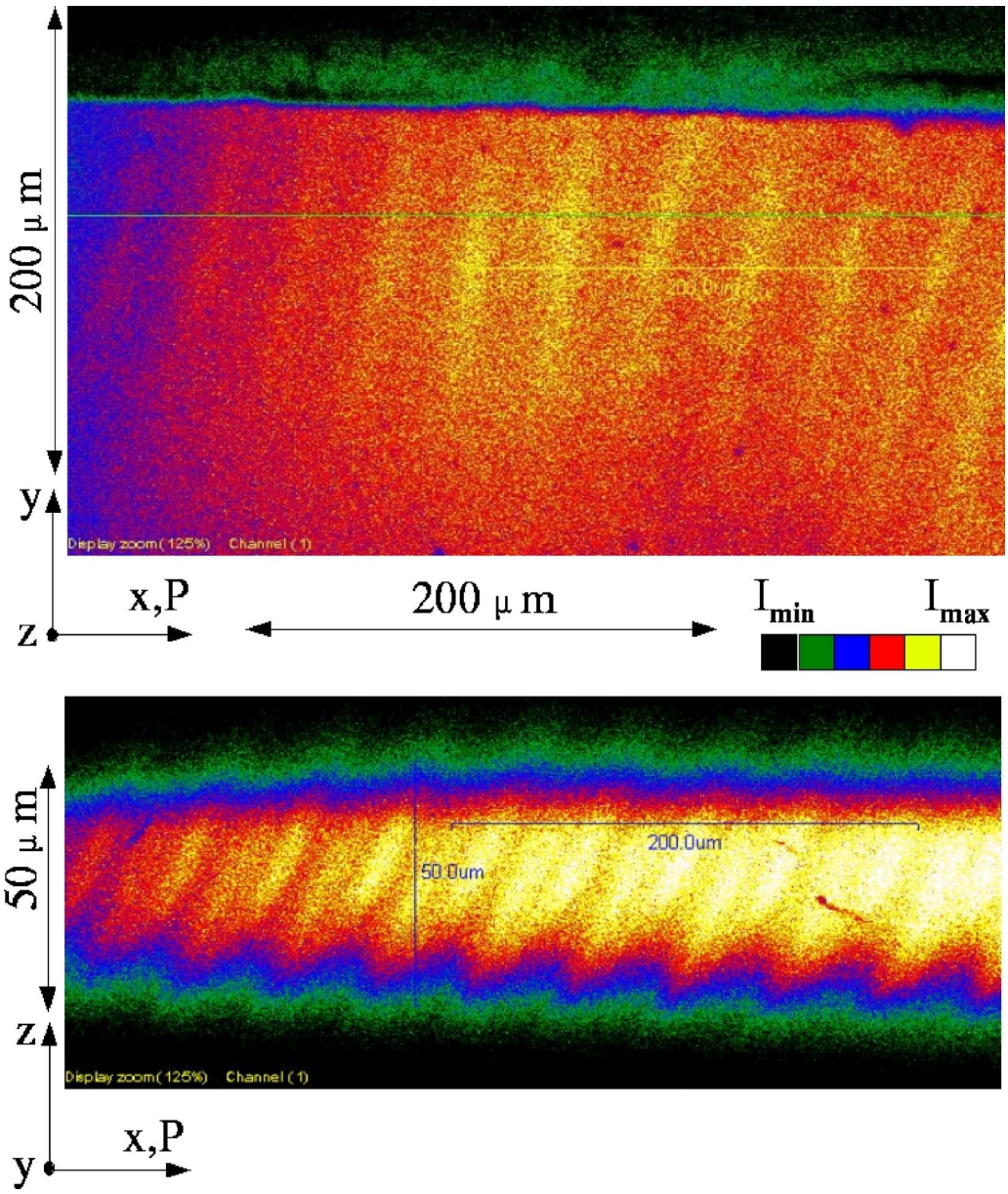

FIG. 3. (Color online) FCPM of normal rolls. At a frequency $f=10$ Hz, the applied square ac voltage is $V=8.10$ V. The threshold voltage was $V_{th}=7.98$ V.

light. The dye concentration was chosen such that the fluorescent signal would be strong enough to give sufficient information about localization of convective patterns. On the other hand, the level of doping was chosen well below the solubility limit. Increasing the concentration of the fluorophore molecules will increase the fluorescence signal as long as these molecules do not get too close together. When fluorophore molecules are within a few nanometers of each other they begin to quench each other. Proximity-induced energy or charge transfer between fluorophores multiplies the efficiency of the quenchers [42]. The fluorescence lifetime for BTBP dye is $\tau_f=3.7-3.9$ ns, smaller than the characteristic time of rotational diffusion $\tau_d \sim 10$ ns [37,43]; therefore the dye orientation is not changed during the absorption-emission sequence. BTBP molecules absorb laser light and then relax to the ground state by fluorescence or by nonradi-

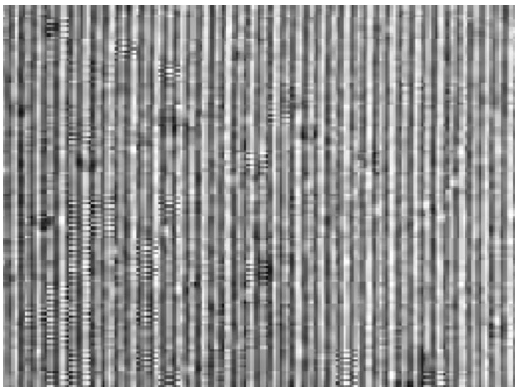

FIG. 4. Shadowgraph image of normal dielectric rolls. The image size is 177×133 μm^2.

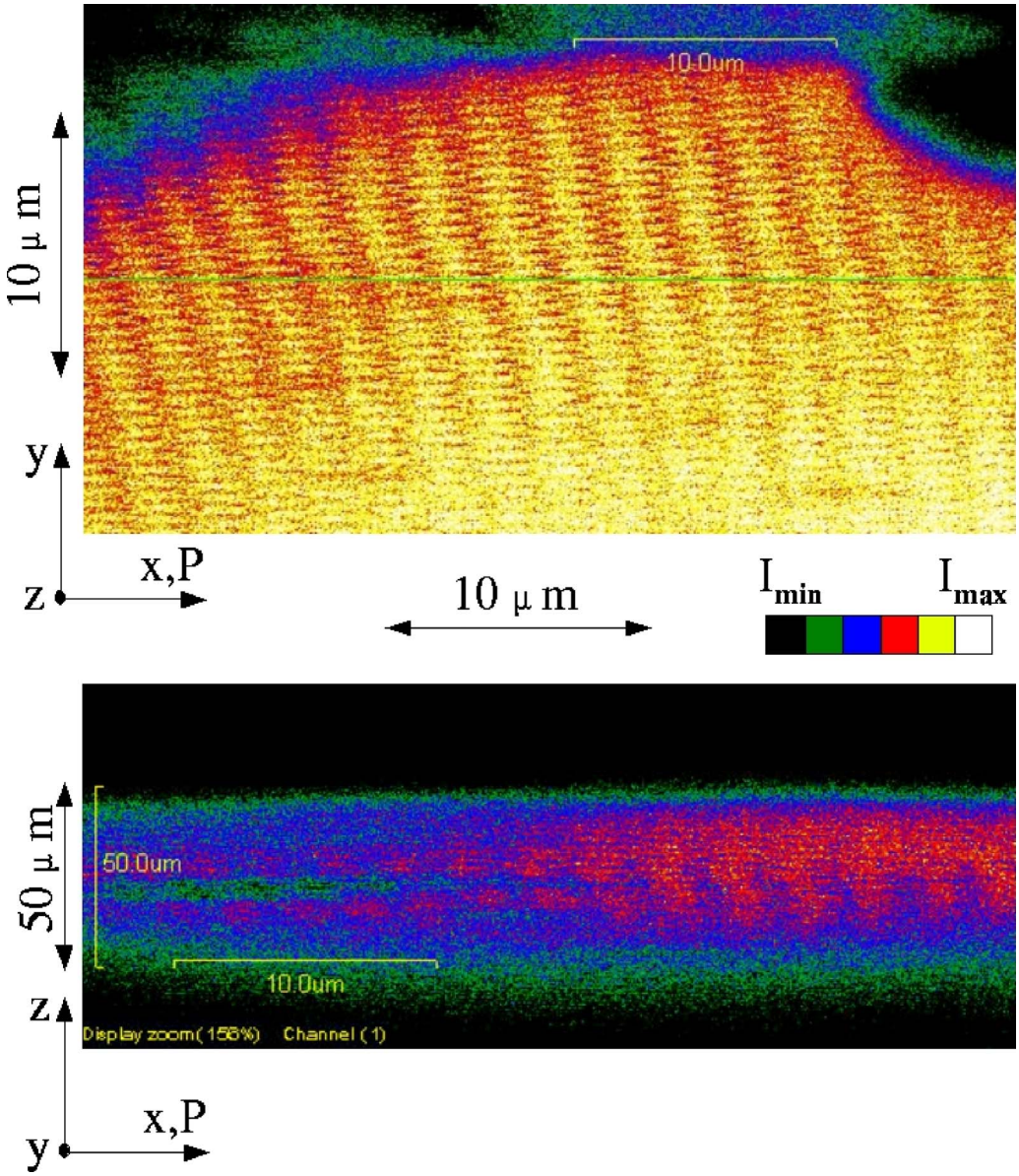

FIG. 5. (Color online) FCM of two layers of normal dielectric rolls, located one at each electrode. The applied square ac voltage is $V=28.9$ V at a frequency $f=60$ Hz. The threshold voltage was $V_{th}=28.8$ V.

ative internal conversion. The Stokes shift is given by the difference between the wavelength of the fluorescence light and that of the absorbed light. Since the spectral absorption dipole is along the long axis of the BTBP molecule, there is a maximum absorption when the polarization of light is along the same direction. The intensity of the fluorescence signal when the input light is polarized has the dependence $I \sim \cos^4 \beta$, where β is the angle between the direction of light polarization and the director **n** [36,37,44].

The NLC was confined between two indium tin oxide–coated glass substrates: one 1.1 mm thick, and the other only 0.17 mm thick [45]. Homogeneous alignment (along x) for the nematic director was achieved by rubbing the polyimide (PI2555) coating of the glass substrates. The two substrates were assembled with their coating alignment antiparallel to each other. The obtained LC cell was placed on the microscope stage with the thin substrate at the top, such that the laser beam would enter first through this substrate, thus giving optimal resolution for the FCPM images. The gap d between the two glass electrodes was chosen large enough for a separation of dielectric rolls to be seen. At the same time, the value of d was limited by the axial defocusing of the two propagating modes (extraordinary and ordinary) of the laser beam in the anisotropic LC [36,37]:

$$\Delta z = g(\Delta n/n_{av})z \tag{2}$$

where g is a dimensionless coefficient of the order of unity that depends on the geometry of light propagation, $\Delta n = n_e - n_o$ is the birefringence of the anisotropic medium, with n_e and n_o the indices of refraction for the extraordinary and the ordinary ray, respectively, and z is the depth of scanning. The average index of refraction n_{av} is evaluated as

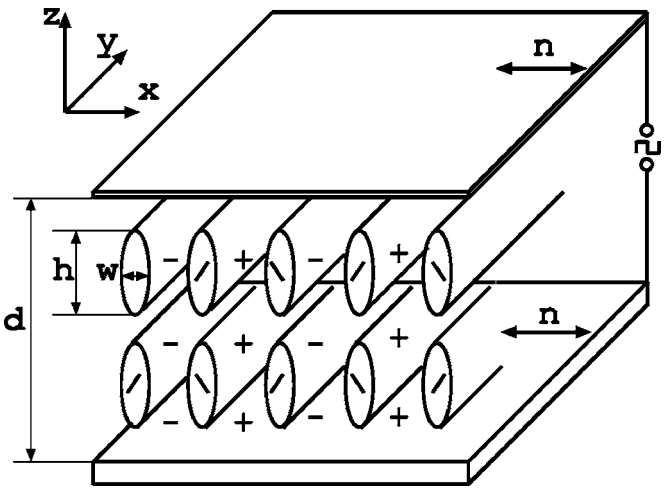

FIG. 6. Model for the fluid flow in the normal dielectric mode. The space charge is stationary.

$$n_{av} = \frac{2n_o + n_e}{3}. \tag{3}$$

The lower the birefringence Δn of the material and (or) the smaller the depth z of scanning, the better the resolution of the FCPM image. For Mischung 5, the birefringence Δn drops from 0.147 at 15.5 °C to 0.082 at 68.5 °C [40]. The advantage for the in-depth resolution of using the small birefringence of the material at high temperatures was not taken. First, the stabilization of NDRs was possible only at low temperatures, where the viscosities were higher, although the birefringence was also larger. Second, and most important, was the necessity to lower the threshold for the dielectric mode below the threshold for the isotropic mode. The results presented here were obtained at $T=15.0$ °C, for which the cutoff frequency was $f_c=16$ Hz. At $T=15.5$ °C, the indices of refraction are $n_e=1.6438$ and $n_o=1.4968$ [40], respectively. The cell gap $d=31.1\pm0.1$ μm was found using a Perkin-Elmer uv-visible spectrometer, model Lambda 18. For this thickness of the slab and the numerical aperture of the microscope objective 0.6, the axial defocusing [Eq. (2)] was $\Delta z\sim 3$ μm. Nevertheless, the depth of the NDRs was expected to be several times this value. The cells filled with the Mischung-BTBP mixture by capillary action were heated above the clearing point (~84 °C) in order to remove imperfections in the alignment. The phase diagram of EHIs (threshold voltage as a function of frequency) has been described elsewhere [38,39]. The condition stated by Eq. (1) was well satisfied for the observation of normal rolls in the dielectric mode.

The experimental setup is shown in Fig. 2. The excitation beam given by a 488 nm air-cooled argon ion laser was polarized and then focused by a dry objective, having magnification 40× and numerical aperture (NA) 0.6, into a submicrometer volume (voxel) of the sample. The condenser NA was adjusted to 0.5, the required 80% value from the NA of the objective [42]. The fluorescence light passed through a pinhole which, by its small size, discriminated between regions below and above the voxel under observation. In order to obtain a well-resolved in-depth scan, the size of the pinhole passed by the fluorescence light was adjusted to 100 μm. The magnification and the numerical aperture of the objective determined this value. A photomultiplier tube (PMT1) detected the fluorescent light in the spectral region 510–550 nm. The laser power was small (~300 nW), in order to avoid light-induced orientation of the dye-doped material [46]. High level of the excitation caused by the laser heating of the sample can also induce nonlinear effects [47]. Another effect due to laser heating of the sample is a decrease in the threshold voltage for EHI. Both horizontal xy and in-depth xz scans were obtained. The intensity of the amplified fluorescence signal was stored in the computer as xy or xz thin optical slices. Transmitted textures were detected by a second multiplier (PMT2, spectral region 585–610 nm), although the optical microscope was preferred for the quality of the shadowgraph images. When scanning NRs, a polarizer was used, with its optical axis parallel to the director alignment. No polarizer was used for scanning NDRs. More precisely, when FCPM was used for scanning NDRs, the mapping intensity was too low to permit image analysis. The reason is the small dye concentration correlated with the small scale of the scans. We have used, therefore, fluorescence confocal microscopy (FCM) to image NDRs. The temperature of the sample was stabilized within ±0.05 °C with the RM6 Lauda Brinkmann temperature controller. A square ac voltage across the sample was applied using a Standard Research Systems DS345 function generator, amplified by a model 7602 wideband amplifier, and measured with a Keithley 2000 multimeter.

III. RESULTS

Before revealing the dielectric mode we scanned NRs, recognized from the beginning [48] as a bulk instability. FCPM scans both in the layer plane (xy) and in the transverse plane (xz) were obtained (Fig. 3). Minimum fluorescence intensity (color mapping, black) corresponds to the location of cell substrates. In between, maximum fluorescence intensity (color mapping, yellow-white) corresponds to the unperturbed director, since the transition moment of the dye molecules, being parallel to the director, is also parallel to the direction of polarization of the input light. As see on the xz FCPM scan, the fluid-flow pattern extends from one electrode to the other as a bulk layer of rolls, which are known to be counter-rotating vortices associated with the director pattern. The oblique orientation of the rolls with respect to the cell normal is due to the difference in the attributes of the two glass substrates, one being thinner than the other. When voltage is applied across the cell, the thin substrate is bent increasingly from the glued edges to the middle of the cell. The rolls being normal to the director and thus also to the substrates, they tilt with respect to their direction in the absence of an applied voltage (also the direction of the cell normal). On the scans, this effect is more pronounced in the case of large-scale convection (NRs) and not really discrimated in the case of small-scale convection (NDRs). The undulating regions more emphasized near the bottom electrode are due to light focusing at the locations of

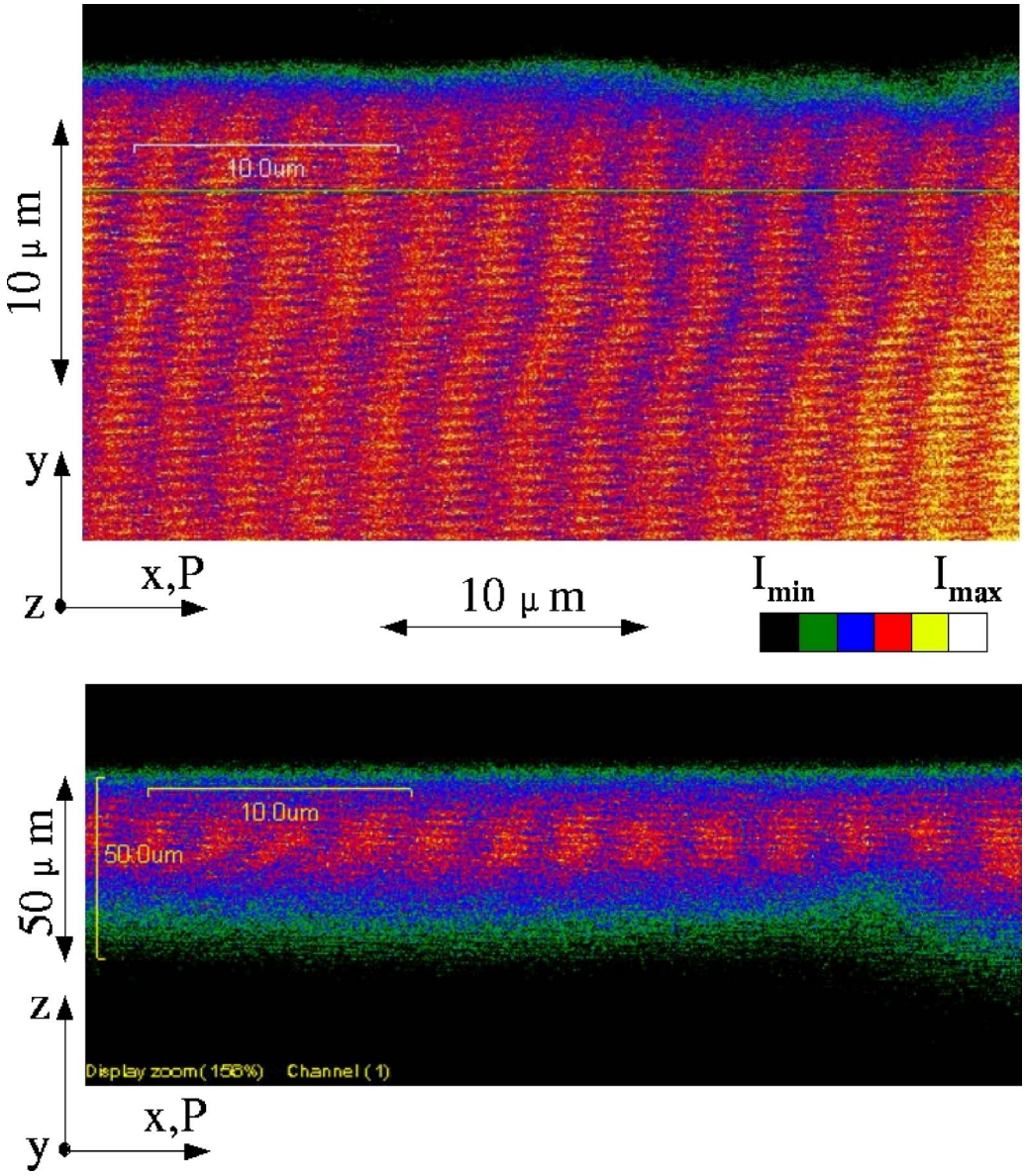

FIG. 7. (Color online) FCM of one layer of dielectric rolls. The applied square ac voltage is $V=33.1$ V at a frequency $f=60$ Hz.

unperturbed director. The available region for light focusing is larger at the bottom substrate (toward the laser light source) than at the upper substrate. The counter effect is light absorbtion and increased defocusing near the bottom electrode. These two effects make the image asymmetric along the z axis. Above the threshold for the dielectric mode, the shadowgraph observation shows the NDR pattern very similar to Williams-Kapustin domains, except for the very low contrast and also the very small wavelength not scaling with the cell gap (Fig. 4). FCM scans revealed convective layers located one at each electrode (Fig. 5). The xz scan shows that the NDR instability develops first at the electrodes as small-scale flow. Strong anchoring makes director oscillations difficult and charges accumulate by the CH mechanism. In the cell middle, about 5–8 μm from the 31 μm cell gap, the intensity of the fluorescence mapping shows a minimum. That is nothing else but a reflection of the fast oscillation of the director with the frequency of the driven voltage and, at the same time, an indication of the absence of any flow pattern. Since FCM and not FCPM was used, regions with higher fluorescence intensity must have higher dye concentration. We expect these regions to be also characterized by slower dynamics. Therefore, the lower fluorescence intensity in the cell middle should indicate a fast dynamics of the LC director. Moreover, if the cell middle were convection-free, we would see higher fluorescence intensity with FCPM, but this did not happen. This situation is schematically described in Fig. 6. As Fig. 5 shows, nonuniform fluid flow is also manifested in the layer plane by the coexistence of two-layer and one-layer convection, which was attributed to the high sensitivity of the EHI to the local heating given by the laser beam. The roll width w is about 2–3 μm, while its depth h is about 10–13 μm. This gives a ratio of roll width to cell gap ranging from 10 to 16. At finite distance from the threshold, the convection filled the cell in only one layer of elongated rolls (Fig. 7), as the Orsay Liquid Crystal Group predicted

[48]. Increasing even more the applied voltage, the chevron pattern set in. While the in-plane transmission scan revealed the defect-mediated chevron pattern, both the in-plane and in-depth FCPM scans showed the absence of any director or flow pattern. The chevron pattern is clearly the optical image of the director fast oscillation and, therefore, cannot be detected by the FCPM scans.

IV. DISCUSSION AND CONCLUSION

As first observed for chevrons [25,28], our observations found that NDRs too are flow patterns and not the result of bending oscillation of the director. We observed this in a not very thick cell, while previously reported optical observations used thick cells too [26]. The SM can explain the transition from bulk to surface NDRs for the lower limit of the intermediate-frequency range. Our observations are compatible with this case. A transition at high frequencies cannot be explained by the SM. The high-frequency range was not investigated due to limitations in both temporal and spatial resolutions for the confocal technique. It would have been very interesting, though, to observe the previously reported [31] saturation of wavelengths to 2 μm that does not agree with the predicted continuous decrease with the frequency $\sim 1/\sqrt{f}$.

The twist mode about z, also the direction for the applied electric field, plays an important role in the dielectric mode of EHI. The twist is known to be active for the chevron formation that follows the NDRs. As was found in [49], if the anisotropy axis is twisted, the pattern is localized in planes that are parallel to the director. The in-depth extension of the pattern (along z) could be smaller than the cell gap, and therefore breakdown of the bulk properties is expected, as we have indeed observed. The director pattern in the NDR mode must be 3D, in the sense defined in [51], namely, when (i) the spatial period(s) are not determined by the spatial extension of the sample and (ii) the spatial extension of the sample is in all directions large compared to the period(s) of the underlying pattern. EHI with magnetic field parallel to the electric field in NLCs reveals 2D dendritic patterns [10,11], while the shadowgraph imaging shows that the director pattern is 3D. Notice that the conductive mode of the EHI always leads to quasi-2D patterns. The most important thing about 3D director patterns in NLCs is the massive occurrence of homogeneous soft modes [50–52], which couple to the pattern and can drastically change its dynamics [11]. A reduction of the 3D director pattern dynamics to a quasi-2D form, as a result of the interaction of the pattern with the homogeneous twist mode could be tested by measurements of the electric Nusselt numbers [51,53]. Interesting enough, both the EHI dendritic pattern and the NDR pattern have lower dimensionality than the director pattern (3D). The dendritic pattern is 2D, while NDRs represent a 1D pattern. In both cases, the homogeneous twist mode couples to the pattern and changes its dynamics significantly. The highly nonlinear feature of these phenomena explains why there is no theoretical description yet available for convective dendrites and only a partial understanding of the dielectric mode. Combined analytical and numerical methods like those developed in [54], along with more 3D experiments, could bring more understanding of the 3D liquid crystal director patterns and fluid flow, and their feedback to each other.

The dielectric mode of the electrohydrodynamic instability in a nematic liquid crystal was three-dimensionally imaged by fluorescence confocal microscopy as two systems of small-scale convective flow formed at the electrodes. In the middle region, a structureless convection with the director oscillating with the frequency of the applied voltage was observed. The pattern wavelength was more than one order of magnitude smaller than and in no relation to the cell gap. We have also found that, in the normal dielectric mode, a transition from surface to bulk normal dielectric occurs when increasing the amplitude while keeping constant the frequency of the applied voltage. By directly imaging both the director pattern and the flow, our conclusion is that the true dielectric mode is surface flow instability and not a director pattern.

ACKNOWLEDGMENTS

This work was supported by Kent State University and the National Science Foundation, Grant No. DMR-9988614.

[1] P. G. de Gennes and J. Prost, *The Physics of Liquid Crystals* (Clarendon Press, Oxford, 1993).
[2] S. Chandrasekhar, *Liquid Crystals* (Cambridge University Press, Cambridge, U.K., 1992).
[3] N. A. Vaz, G. W. Smith, and G. P. Montgomery, Mol. Cryst. Liq. Cryst. **146**, 1 (1987).
[4] D. Subacius, P. J. Bos, and O. D. Lavrentovich, Appl. Phys. Lett. **71**, 1350 (1997).
[5] G. Panasyuk, J. R. Kelly, P. Bos, E. C. Gartland, and D. W. Allender, Liq. Cryst. **31**, 1503 (2004).
[6] N. Gheorghiu, J. L. West, A. V. Glushchenko, and M. Mitrokhin, Appl. Phys. Lett. **88**, 26 (2006).
[7] J. S. Langer, Rev. Mod. Phys. **52**, 1 (1980).
[8] P. E. Cladis, J. T. Gleeson, P. L. Finn, and H. R. Brand, Phys. Rev. Lett. **67**, 3239 (1991).
[9] G. Zocchi, P. Tabeling, and M. Ben Amar, Phys. Rev. Lett. **69**, 601 (1992).
[10] J. T. Gleeson, Nature (London) **385**, 511 (1997).
[11] N. Gheorghiu and J. T. Gleeson, Phys. Rev. E **66**, 051710 (2002).
[12] M. C. Cross and P. C. Hohenberg, Rev. Mod. Phys. **65**, 851 (1993).
[13] L. Kramer and W. Pesch, in *Pattern Formation in Liquid Crystals*, edited by A. Buka and L. Kramer (Springer-Verlag, New York, 1996).
[14] S. A. Pikin, *Structural Transformations in Liquid Crystals* (Gordon and Breach Science Publishers, Amsterdam, 1991).
[15] L. M. Blinov and V. G. Chigrinov, *Electrooptic Effects in*

Liquid Crystal Materials (Springer-Verlag, New York, 1994).
[16] E. F. Carr, Mol. Cryst. Liq. Cryst. **7**, 253 (1969).
[17] W. Helfrich, J. Chem. Phys. **51**, 4092 (1969).
[18] S. Rasenat, G. Hartung, B. L. Winkler, and I. Rehberg, Exp. Fluids **7**, 412 (1989).
[19] R. Williams, J. Chem. Phys. **39**, 384 (1963).
[20] A. P. Kapustin and L. K. Vistin, Kristallografiya **10**, 118 (1965).
[21] L. M. Blinov, A. N. Trufanov, V. G. Chigrinov, and M. I. Barnik, Mol. Cryst. Liq. Cryst. **74**, 1 (1981).
[22] A. N. Trufanov, L. M. Blinov, and M. I. Barnik, Zh. Eksp. Teor. Fiz. **78**, 622 (1980).
[23] R. Chang, Mol. Cryst. Liq. Cryst. **20**, 267 (1973).
[24] M. I. Barnik, L. M. Blinov, M. F. Grebenkin, and A. N. Trufanov, Mol. Cryst. Liq. Cryst. **37**, 47 (1976).
[25] H. Yamazaki, S. Kai, and K. Hirakawa, J. Phys. Soc. Jpn. **56**, 502 (1987).
[26] S. Kai, K. Yamaguchi, and K. Hirakawa, Jpn. J. Appl. Phys. **14**, 1653 (1975).
[27] R. Chang, J. Appl. Phys. **44**, 1885 (1973).
[28] B. R. Jennings and H. Watanabe, J. Appl. Phys. **47**, 4709 (1976).
[29] L. M. Blinov, M. I. Barnik, and A. N. Trufanov, Mol. Cryst. Liq. Cryst. **89**, 47 (1982).
[30] P. Pieranski and E. Guyon, Phys. Rev. A **9**, 404 (1974).
[31] H. Bohatsch and R. Stannarius, Phys. Rev. E **60**, 5591 (1999).
[32] H. Miike, Y. Kuriyama, H. Hashimoto, and Y. Ebina, J. Phys. Soc. Jpn. **53**, 3280 (1984).
[33] P. A. Penz and G. W. Ford, Phys. Rev. A **6**, 414 (1972).
[34] M. I. Barnik, L. M. Blinov, S. A. Pikin, and A. N. Trufanov, Zh. Eksp. Teor. Fiz. **72**, 756 (1977).
[35] E. Bodenschatz, W. Zimmermann, and L. Kramer, J. Phys. (France) **49**, 1875 (1988).
[36] I. I. Smalyukh, S. V. Shiyanovskii, and O. D. Lavrentovich, Chem. Phys. Lett. **336**, 88 (2001).
[37] S. V. Shiyanovskii, I. I. Smalyukh, and O. D. Lavrentovich, in *Defects in Liquid Crystals: Computer Simulations, Theory and Experiments*, edited by O. D. Lavrentovich, P. Pasini, G. Zannoni, and S. Žumer, NATO Advanced Study Institute, Series II: Mathematics, Physics, and Chemistry (Kluwer Academic Publishers, Dordrecht, 2001), Vol. 43.
[38] H. Amm, M. Grigutsch, and R. Stannarius, Mol. Cryst. Liq. Cryst. Sci. Technol., Sect. A **320**, 11 (1998).
[39] J. Shi, C. Wang, V. Surendranath, K. Kang, and J. T. Gleeson, Liq. Cryst. **29**, 877 (2002).
[40] R. Stannarius (private communication).
[41] A. J. Bur, S. C. Roth, and C. L. Thomas, Rev. Sci. Instrum. **71**, 1516 (2000).
[42] *Handbook of Biological Confocal Microscopy*, 2nd ed., edited by J. B. Pawley (Plenum Press, New York, 1995).
[43] W. E. Ford and P. V. Kamat, J. Phys. Chem. **91**, 6373 (1987).
[44] I. I. Smalyukh and O. D. Lavrentovich, Phys. Rev. E **66**, 051703 (2002).
[45] Bioptechs Inc., Butler, Pennsylvania.
[46] I. Janossy, Phys. Rev. E **49**, 2957 (1994).
[47] H. J. Yuan, L. Li, and P. Palffy-Muhoray, Mol. Cryst. Liq. Cryst. **199**, 223 (1991).
[48] Orsay Liquid Crystal Group, Phys. Rev. Lett. **25**, 1642 (1970).
[49] A. G. Rossberg, Phys. Rev. E **62**, 4682 (2000).
[50] E. Plaut and W. Pesch, Phys. Rev. E **59**, 1747 (1999).
[51] A. G. Rossberg, Phys. Rev. E **62**, 8114 (2000).
[52] B. Dressel, A. Joets, L. Pastur, W. Pesch, E. Plaut, and R. Ribotta, Phys. Rev. Lett. **88**, 024503 (2002).
[53] J. T. Gleeson, N. Gheorghiu, and E. Plaut, Eur. Phys. J. B **26**, 515 (2002).
[54] G. Panasyuk and D. W. Allender, J. Appl. Phys. **91**, 9603 (2002).